Bioorganic Chemistry 86 (2019) 210–223

Contents lists available at ScienceDirect

Bioorganic Chemistry

journal homepage: www.elsevier.com/locate/bioorg

Synthesis of substituted biphenyl methylene indolinones as apoptosis inducers and tubulin polymerization inhibitors

Kavitha Donthiboina[a], Pratibha Anchi[b], P.V. Sri Ramya[a], Shailaja Karri[b], Gannoju Srinivasulu[a], Chandraiah Godugu[b], Nagula Shankaraiah[a,*], Ahmed Kamal[a,c,*]

[a] Department of Medicinal Chemistry, National Institute of Pharmaceutical Education and Research (NIPER), Hyderabad 500 037, India
[b] Department of Regulatory Toxicology, National Institute of Pharmaceutical Education and Research (NIPER), Hyderabad 500 037, India
[c] School of Pharmaceutical Education and Research (SPER), Jamia Hamdard, New Delhi 110062, India

ARTICLE INFO

Keywords:
Methylene indolinones
Cytotoxicity
Tubulin polymerization
Cell cycle
Annexin binding
Molecular modeling

ABSTRACT

A new series of biphenyl methylene indolinones has been designed, synthesized and evaluated for their *in vitro* antiproliferative activity against various cancer cell lines like DU-145 (prostate cancer cell line), 4T1 (mouse breast cancer cell line), MDA-MB-231 (human breast cancer cell line), BT-549 (human breast cancer cell line), T24 (human urinary bladder carcinoma cell line), and HeLa (cervical cancer cell line). Among the series, compound **10e** showed potent *in vitro* cytotoxic activity against HeLa and DU-145 cancer cell lines with IC_{50} value of 1.74 ± 0.69 μM and 1.68 ± 1.06 μM respectively. To understand the underlying mechanism of most potent cytotoxic compound **10e**, various mechanistic studies were carried out on DU-145 cell lines. Cell cycle analysis results revealed that these conjugates affect both G0/G1 and G2/M phase of the cycle, tubulin binding assay resulted that compound **10e** interrupting microtubule network formation by inhibiting tubulin polymerization with IC_{50} value of 4.96 ± 0.05 μM. Moreover, molecular docking of **10e** on colchicine binding site of the tubulin explains the interaction of **10e** with tubulin. Clonogenic assay indicated inhibition of colony formation by compound **10e** in a dose dependent manner. In addition, morphological changes were clearly observed by AO/EB and DAPI staining studies. Moreover, ROS detection using DCFDA, JC-1, and annexin V-FITC assays demonstrated the significant apoptosis induction by **10e**.

1. Introduction

Microtubule dynamics is an attractive biological target for various synthetic and semi-synthetic chemotherapeutic agents [1,2] as microtubule system is ubiquitous element, serves as primary substrate for various cellular processes such as cell division, formation, maintenance of cell shape, regulation of motility, cell signaling, secretion and intracellular transport [3]. Anti-microtubule agents can interrupt highly dynamic microtubule net work and they are categorized as microtubule stabilizing agents, vinca site binding agents and colchicine site binding agents [4]. Most of the studies revealed that biphenyl configuration is an essential dimension to mimic colchicine binding site, the presence of planar group is one of the pharmacophoric features required to bind colchicine site of the tubulin [5a], which is present in several cytotoxic natural products such as steganacine (**1**), steganone (**2**), eupomatilone (**3**), and buflavine (**4**, Fig. 1) [5b].

On the other hand, oxindole is a privileged scaffold exhibiting potential biological activities like anticancer, antibacterial, antifungal, antiviral and anti-angiogenic properties [6,7]. Sunitinib (**5** SU11248, Fig. 1) having 3-alkenyl oxindole part is significant as orally active receptor tyrosine kinase (RTK) inhibitor, currently prescribed for the treatment of renal cell carcinoma and gastrointestinal stromal tumours [8,9]. Semaxanib (**6**, SU5416) is a related anticancer, anti-angiogenic scaffold which is in clinical trials for colorectal cancer [10]. A-432411 is also an another oxindole containing anti-microtubule agent, which activate spindle check points to induce apoptosis [11]. Based on these investigations by exemplifying the significance of biaryl compounds and oxindole derivatives with potent cytotoxic property, herein we have developed a new series of biaryl moieties which are in conjugation with 3-alkenyl oxindole (Fig. 2). In recent years, molecular hybridization approach is an essential tool in medicinal chemistry which involves combining of two bioactive scaffolds [12]. Previously, our research group reported hybridization of bioactive moieties like imidazo-thiazoles, 2-anilinopyrydyls and pyrazoles with oxindole which were

* Corresponding authors at: Department of Medicinal Chemistry, National Institute of Pharmaceutical Education and Research (NIPER), Hyderabad 500 037, India (A. Kamal).
E-mail addresses: shankar@niperhyd.ac.in (N. Shankaraiah), ahmedkamal@iict.res.in (A. Kamal).

https://doi.org/10.1016/j.bioorg.2019.01.063
Received 19 September 2018; Received in revised form 17 January 2019; Accepted 27 January 2019
Available online 29 January 2019
0045-2068/

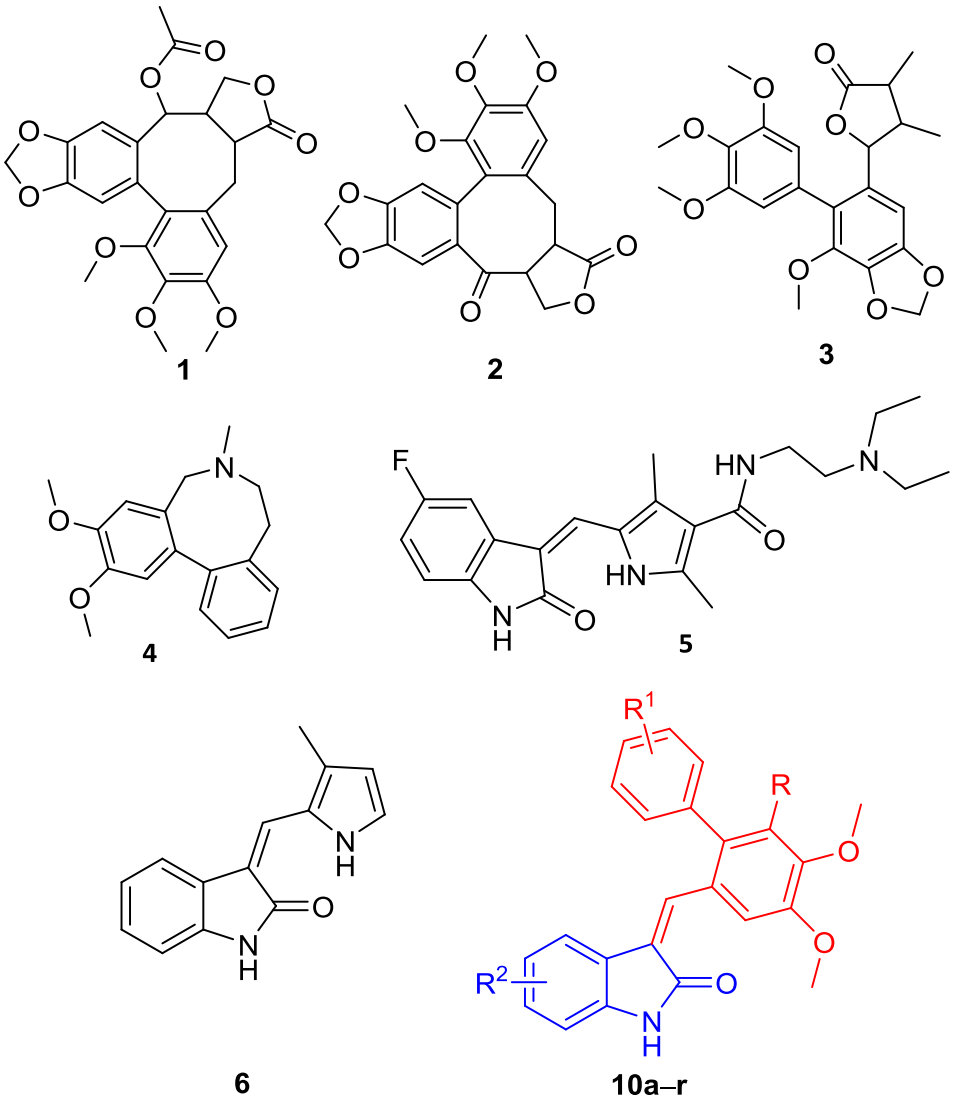

Fig. 1. Chemical structures of bioactive steganacine (**1**), steganone (**2**), eupomatilone (**3**), buflavin (**4**), sunitinib (**5**), semaxinib (**6**), and newly synthesized biphenyl methylene indolinones **10a–r**.

evaluated and reported as anti-cancer agents [13–15]. In continuation of our efforts towards the synthesis of bioactive scaffolds, herein we attempted to link 3-alkenyl oxindoles with biphenyl moiety which result in biphenyl methylene indolinones **10a–r** and further evaluated for their *in vitro* anti-cancer activity.

The syntheses of target biphenyl methylene indolinones **10a–r** were depicted in Scheme 1, thus includes bromination of substituted benzaldehydes **7a**,**b** using Br_2 which resulted **8a**,**b** followed by Suzuki cross-coupling with $Pd(PPh_3)_4$ afforded the key biphenyl 2-carbaldehyde intermediates **9a–d** in overall good yields. Finally, the target compounds **10a–r** were obtained by the Knoevenagel condensation between different oxindoles **11a-e** and biphenyl 2-carbaldehyde **9a–d** in the presence of piperidine. These compounds were obtained as mixture of *E/Z* isomers in the ratio of 9:1. Major isomer *E* was isolated by conventional column chromatography and confirmed by using NMR spectroscopy. Moreover, NOE results confirmed *E* as major product by assigning the conformation of representative compound **10e**. To know all proton resonances, ^{1}H NMR of compound **10e** was carried out using gDQFCOSY and ROESY experiments in DMSO-d_6 at 30 °C. NOE was observed between H1-H2, H4-H6, H4-OMe7 and a very weak interaction was observed between H3-OMe7 in ROESY experiment explains the geometry of double bond and the configuration of **10e** was characterized as *E*-isomer as depicted in Fig. 3.

1.1. Cytotoxicity assay

The synthesized compounds **10a–r** were evaluated for their *in vitro* cytotoxicity by dimethylthiazol-2-yl)-2,5-diphenyltetrazolium bromide (MTT) assay [16] against a panel of selected cancer cell lines, viz., DU-145 (prostate cancer cell line), 4T1 (mouse breast cancer cell line), MDA-MB-231 (human breast cancer cell line), BT-549 (human breast cancer cell line), T24 (human urinary bladder carcinoma cell line), HeLa (human cervical cancer) and compared with reference compound vincristine sulfate (Table 1). Among the synthesized compounds, **10e** showed significant cytotoxic activity on all the tested cancer cell lines, and a potent effect on DU-145, and HeLa cell lines with an IC_{50} value of 1.68 ± 1.06 and 1.74 ± 0.69 μM, respectively. Compounds **10b–d** showed effective cytotoxicity against DU145 cell line; however compounds **10a**, **10g**, **10i**, **10k**, **10l**, **10m**, **10o** and **10p** showed moderate cytotoxicity without the selectivity on different cancer cell lines. Compounds **10f**, **10j**, **10n**, **10q** and **10r** were found to be inactive at the tested conc. of 50 μM (IC_{50} > 50 μM, not included in Table 1) against all the tested cell lines.

Structure activity relationships (SARs) can be exemplified by using various substitutions on ring A, B and C (Fig. 4). From the preliminary screening results, it was observed that most of the compounds are showing potent to moderate cytotoxicity on tested cancer cell lines.

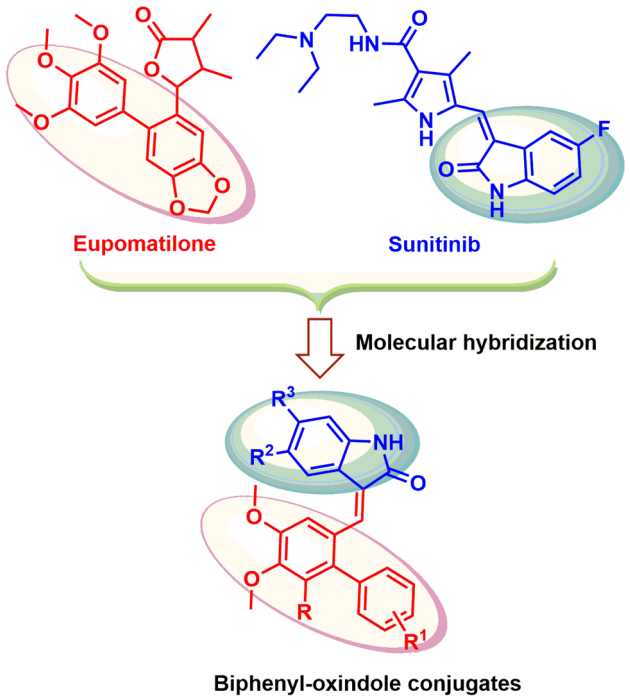

Fig. 2. Design of biphenyl-oxindole conjugates *via* molecular hybridization approach.

Based on the results in Table 1, it is noted that compounds **10b–e** showed significant activity compared to other compounds in this series, it was showed that OCH_3 substitution at 3rd position of ring A, and presence of F at the 4th position of ring B responsible for the activity. Compound **10e** which is having Cl atom on 6th position of ring C is most potent on all the tested cancer cell lines, other compounds **10b-d** having substitution at 5th position of ring C were more selective towards prostate (DU-145) and cervical cancer (HeLa) cell lines, whereas compound **10a** not having any substitution on ring C is almost less active. The compounds **10g** and **10h** having F atom at ring B was shifted from 4th position to 3rd position, potency of compounds was lowered and shifted more likely to cervical cancer cell lines. It was notified that when OMe group of ring A was replaced with H, cytotoxic property of compounds **10k–m** was decreased. When modifications were carried out on both A and B rings in the case **10o** and **10p** activity was observed only on DU-145 cell line and inactive against remaining tested cell lines. Most of the compounds were more likely potent towards prostate cancer (DU-145) cell lines compared to other tested cell lines, hence with most potent compound **10e** further mechanistic studies were performed against DU-145 cell line.

1.2. Determination of cell morphology

To evaluate the effect of compound **10e** on morphology and viability of cells, microscopic examination was carried out using phase contrast microscope, by the treatment of compound **10e** on DU-145 cells for 48 h, at concentrations of 1, 2 and 4 μM. Phase contrast imaging resulted that as the concentration of the compound increased there was a clear cut decrease in cell viability with significant morphological changes such as cell shrinkage (Fig. 5). These results indicated that compound **10e** induced distinctive morphological changes and affected viability of the DU-145 cells.

1.3. DAPI staining study

DAPI is a fluorescent stain binds to A-T rich sequence of nucleic acid in rigid manner by which nuclear damage through chromatin condensation can be observed [17]. This happened because of efficiency of DAPI stain diffusion into cell membrane based on the integrity, i.e. stain penetrates with less efficiency into the intact cell membrane when compared to the disintegrated cell membrane it differentiate the normal and apoptotic cells by forming a fluorescent complex with the chromatin. To evaluate the compound **10e** induced nuclear changes in the DU-145 cells DAPI staining was used. This study revealed that, the nuclear structure of control cells was intact with round shape, while compound 10e treated DU-145 cells showed condensed and micronuclei formation along with some horse-shoe shaped nuclei in a dose depended manner (Fig. 6) indicating the extent of apoptosis.

1.4. Acrdine orange/ethidium bromide staining

Acridine orange (AO)/Ethidium bromide (EB) is also a fluorescent dye that can differentiate between live, apoptotic and necrotic cells. The underlying mechanism is AO has an ability to permeate through the intact cell membrane and stains nuclei green in colour, while EB can penetrate through cells which have lost membrane integrity, and stain the nuclei red in colour. After performing this assay, it was notified that control cells displayed normal homogenous morphology and appeared cells green in colour. However upon treatment with compound **10e**, it was clearly visualized that compound induced morphological changes like cell membrane blebbing, and apoptotic body formations (Fig. 7) in a dose dependent manner.

1.5. Measurement of reactive oxygen species (ROS)

Most of the cytotoxic compounds possess a property of ROS generation [18], where it initiates oxidative damage to the mitochondrial membrane potential and permeability. This property can aggravate the process of apoptosis. We evaluated the effect of compound **10e** on ROS generation by DCFDA (2′-7′-dichlorofluorescin diacetate) assay. DCFDA is a fluorogenic dye measures hydroxyl, peroxyl, and other reactive oxygen species (ROS) within cell. The activity initiates after diffusion of dye into the cell where it gets deacetylated by cellular esterases to a non-fluorescent compound, later oxidized by ROS into highly fluorescent 2′, 7′ - dichlorofluorescein (DCF). The corresponding fluorescence intensity displays the extent of generation of ROS. In line with previous experiments, compound **10e** has shown dose dependence in ROS generation also (Fig. 8). Approximately 2 fold increase in fluorescence was emitted in the highest dose treated prostate cancer DU-145 cells.

1.6. Determination of mitochondrial membrane potential

One of the distinctive features of the early stages of programmed cell death is the disruption of active mitochondria. This mitochondrial disruption includes changes in the membrane potential and alterations in the oxidation–reduction potential. To evaluate the effect of compound **10e** on mitochondrial membrane-permeable, JC-1 dye based assay was performed. With this study we have observed a dose dependent increase of J-monomers (disrupted mitochondria cells) formed from normal polarised J aggregate (Fig. 9**)**. This analysis was represented as P1 (normal cells) and P2 populations (polarised cells).

1.7. Annexin V-FITC/propidium iodide staining assay

To quantify the apoptotic effect of compound **10e**, Annexin V-FITC/Propidium Iodide staining assay was carried out [19]. This study facilitates the detection of live cells (Q1-LL; AV−/PI−), early apoptotic cells (Q2-LR; AV+/PI−), late apoptotic cells (Q3-UR; AV+/PI+) and necrotic cells (Q4-UL; AV−/PI+). This assay reveals that compound **10e** has shown apoptosis in a dose dependent manner with an increment in late apoptotic cells [control (0%), at 2.5 μM (7.3%), at 5 μM

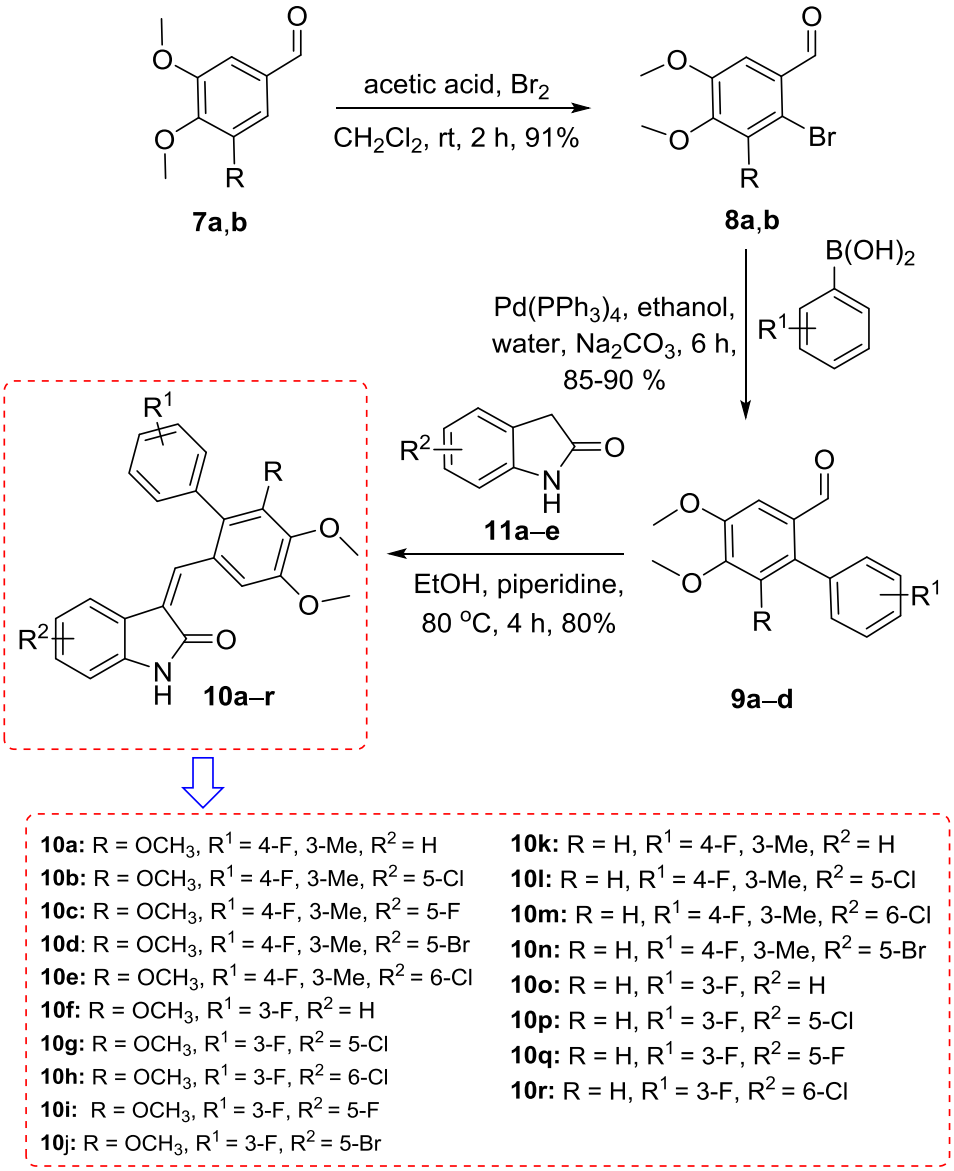

Scheme 1. Synthetic strategy for biphenyl methylene indolinones **10a–r**.

(19.6%) and at 10 μM (20.9%)] (Fig. 10).

1.8. Clonogenic assay

As cancer cells proliferate from a single cell to solid tumours by forming colonies, inhibition of colony formation was considered as an important property of anti-cancer molecule, compound **10e** was evaluated by clonogenic assay to asses its effect on the colony formation. This study proved that **10e** was effective in inhibiting the colony formation even at a low concentration and maximum colonies disappeared at high dose i.e 2.5 μM (Fig. 11).

1.9. Flow cytometric analysis

In vitro screening results proved that compound **10e** has shown eloquent cytotoxic effect therefore the effect of compound **10e** on cell cycle progression was examined by flow cytometric analysis [20–22]. DU-145 cell were treated with 0.5 and 1 μM concentrations of compound **10e**. From Fig. 12, the results clearly explained that **10e** was showing effect on both G0/G1 as well as G2/M in a dose dependent manner, in comparison with control (13.3%) G2/M population at 0.5 μM (13.4%), 1 μM (15.8%) increased, along with this G0/G1 population was also increased control (26%), 0.5 μM (28%), and 1 μM (37%).

1.10. Tubulin polymerization assay

Cytotoxic assay results proved that biphenyl methylene indolinones have anti-proliferative activity against majority of the tested cancer cell lines. It was observed from the literature that most of the alkenyl oxindoles, as well as biphenyl compounds exhibit their cytotoxic activity by inhibiting tubulin polymerization [23] as tubulin is the most critical element for mitosis. To investigate the correlation between cytotoxicity and antimitotic activity, potent compound **10e** was evaluated for tubulin polymerization inhibition in a cell free *in vitro* assay (Fig. 4) using podophyllotoxin as standard. The IC_{50} of compound **10e** was found to be 4.96 ± 0.057 μM by comparing with control. These results indicate that molecular target of these biphenyl methylene indolinones inhibiting the tubulin.

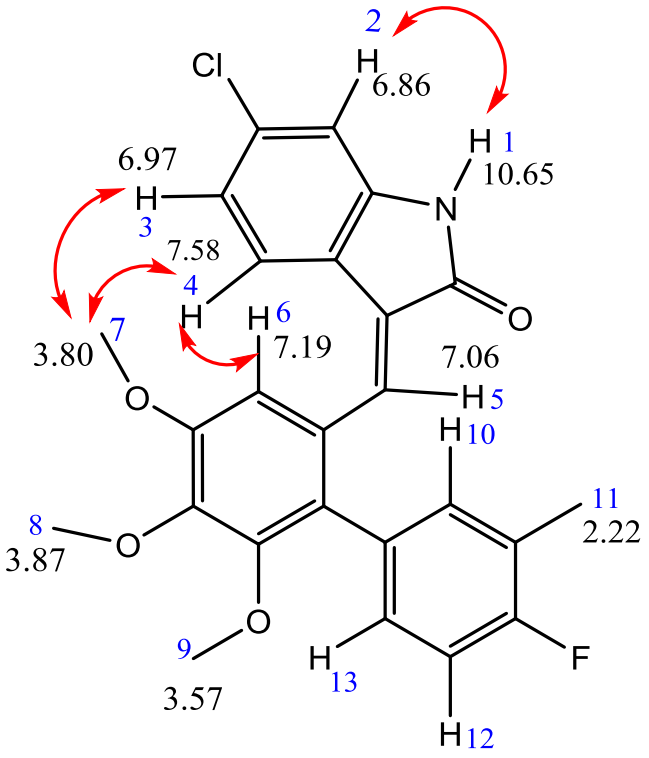

Fig. 3. Schematic representation of characteristic NOEs of compound **10e**.

1.11. Molecular docking simulation study

Molecular docking simulation studies were carried out with the promising compound **10e** in order to understand the mode of binding and type of interactions with the active site of the tubulin (PDB ID: 3E22) [24], by using the GLIDE docking module of Schrödinger suite 2014-3 [25]. Docking study revealed that the top ranked conformation of compound **10e** binds effectively in the colchicine binding site of the tubulin. As can be noticed from the Fig. 13, compound **10e** displayed two hydrogen-bonding interactions with the colchicine-binding domain at the α/β-tubulin interface that appear to play a critical role in binding. The oxygen atom of 4-OMe group on the phenyl ring acts as

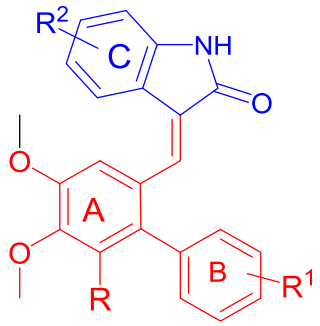

Fig. 4. SAR analysis of biphenyl methylene indolinones.

hydrogen bond acceptor and involved in the hydrogen bond interaction with the side chain NH_2 of Asn101 (d = 1.72 Å). In addition, the oxindole N-H established a hydrogen bond interaction with the back bone carbonyl oxygen of Thr353 (d = 2.11 Å). Moreover, various hydrophobic interactions were noted between **10e** and the active site residues, Ala180, Val181, Tyr224, Leu248, Ala250, Leu255, Met259, Ala316, Ala354, and Val355 that stabilizes the binding of **10e** in the active site cavity of α/β-tubulin interface.

To attain further insight of our findings, we manifested the superimposition of colchicine (the co-crystallized ligand) and the best docked pose of **10e** in the colchicine binding domain at the α/β-tubulin interface. The superimposition poses from Fig. 14 demonstrate that **10e** accommodates in the active site cavity in a similar mode as that of colchicine and evidently, the 3,4,5-trimethoxy phenyl moiety of **10e** superimposes with the trimethoxy phenyl motif of colchicine (see Fig. 15). Altogether, these molecular docking simulation studies furnished a rationalization for the good tubulin polymerization inhibitory activity of **10e**.

2. Conclusion

In conclusion, a series of new biphenyl methylene indolinones **10a–r** was synthesized and evaluated for their *in vitro* cytotoxic potential using a panel of cell lines i.e. DU-145 (prostate cancer cell line), 4T1 (mouse breast cancer cell line), MDA-MB-231 (human breast cancer cell line), BT-549 (human breast cancer cell line), T24 (human urinary bladder carcinoma cell line), HeLa (cervical cancer cell line). Compound **10e** showed potent cytotoxic activity against prostate

Table 1
In vitro antiproliferative activity (IC_{50} value in μM)[a] of compounds **10a–r.**

Compounds	DU-145[b]	4T1[c]	MDA -MB-231[d]	BT549[e]	T24[f]	HeLa[g]
10a	27.71 ± 2.16	8.78 ± 1.67	39.95 ± 1.70	> 50	15.88 ± 4.55	> 50
10b	2.27 ± 0.98	18.40 ± 3.31	> 50	> 50	3.14 ± 1.98	> 50
10c	1.29 ± 1.45	35.56 ± 1.04	27.77 ± 2.16	> 50	> 50	> 50
10d	1.05 ± 1.67	> 50	> 50	> 50	> 50	0.81 ± 0.52
10e	1.68 ± 1.06	13.75 ± 3.61	2.71 ± 1.42	10.02 ± 1.93	2.08 ± 1.75	1.74 ± 0.69
10g	> 50	8.32 ± 0.88	28.9 ± 2.07	> 50	> 50	3.02 ± 1.08
10h	> 50	> 50	> 50	> 50	> 50	16.40 ± 2.53
10i	> 50	21.09 ± 4.04	37.40 ± 1.47	31.77 ± 6.50	> 50	> 50
10k	17.48 ± 2.04	> 50	13.60 ± 3.77	26.91 ± 1.98	6.64 ± 1.77	8.94 ± 1.96
10l	> 50	> 50	> 50	> 50	6.64 ± 4.77	> 50
10m	> 50	> 50	> 50	> 50	35.56 ± 1.56	> 50
10o	7.42 ± 0.63	> 50	> 50	> 50	> 50	> 50
10p	33.24 ± 5.68	> 50	> 50	> 50	> 50	> 50
Vincristine sulfate (nM)	120.22 ± 2.48	ND	107.40 ± 12.07	127.47 ± 0.1	ND	ND

[a] Concentration required for 50% inhibition and mean ± SD of three individual experiments performed in triplicate.
[b] Prostate cancer cell line.
[c] Mouse breast cancer cell line.
[d] Human breast cancer cell line.
[e] Human breast cancer cell line.
[f] Human urinary bladder carcinoma cell line.
[g] Cervical cancer cell line. ND: Not determined.

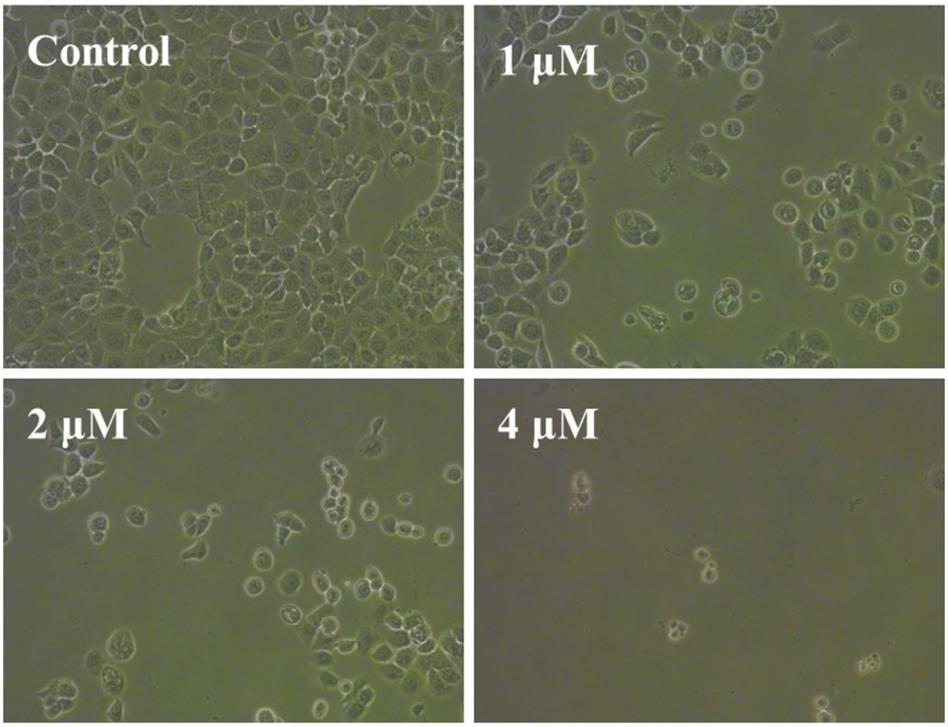

Fig. 5. Phase contrast images of DU-145 cells treated with different concentration of (1, 2, 4 μM) compound **10e** and observed for the compound induced morphological changes at 200× magnification.

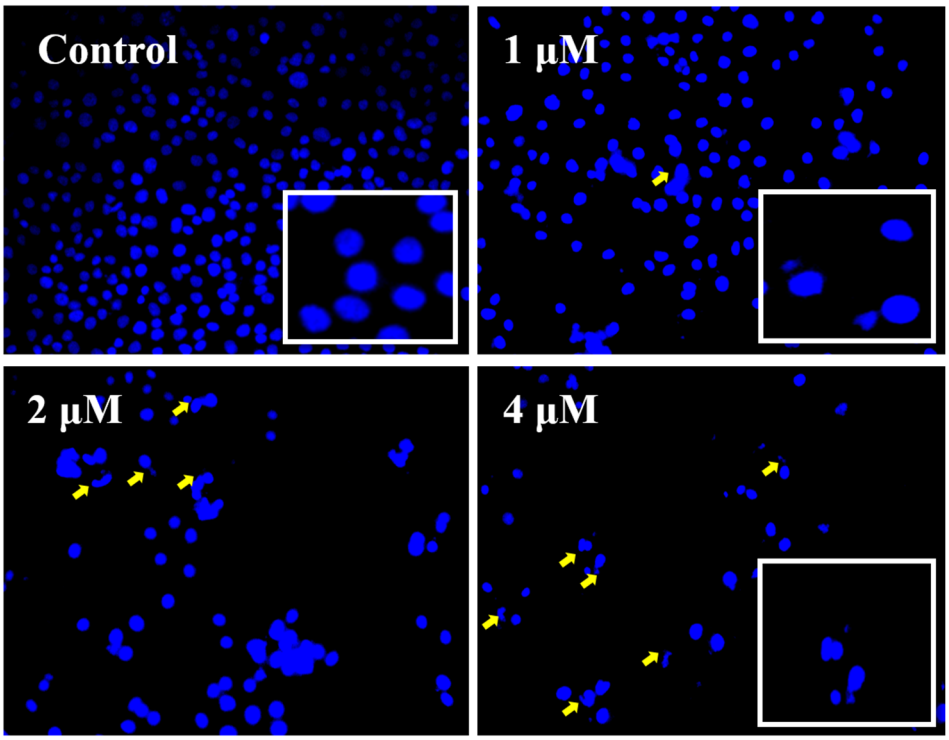

Fig. 6. DAPI stain for nuclear morphology in DU-145 prostate cancer cell lines after 48 h post treatment. The images were taken with fluorescence microscope with a DAPI filter at 200× magnification.

cancer cell line with IC_{50} 1.68 ± 1.06 μM, to evaluate the underlying mechanism with respect to cytotoxicity, various experiments were performed. Tubulin polymerization assay resulted that compound **10e** was able to interfere in mitosis by inhibiting tubulin polymerization; molecular docking also suggested that compound **10e** bind to the colchicine binding site of the tubulin. Flow cytometric analysis revealed that compound **10e** was able to arrest G2/M phase of the cell cycle. Furthermore, compound **10e** induced morphological changes and apoptosis in DU-145 cell lines displayed by acridine orange/ethidium bromide, DAPI staining studies, annexin V-FITC/propidium iodide staining assay, analysis of mitochondrial membrane potential and ROS assays. Moreover clonogenic assay proved that compound **10e** interrupt

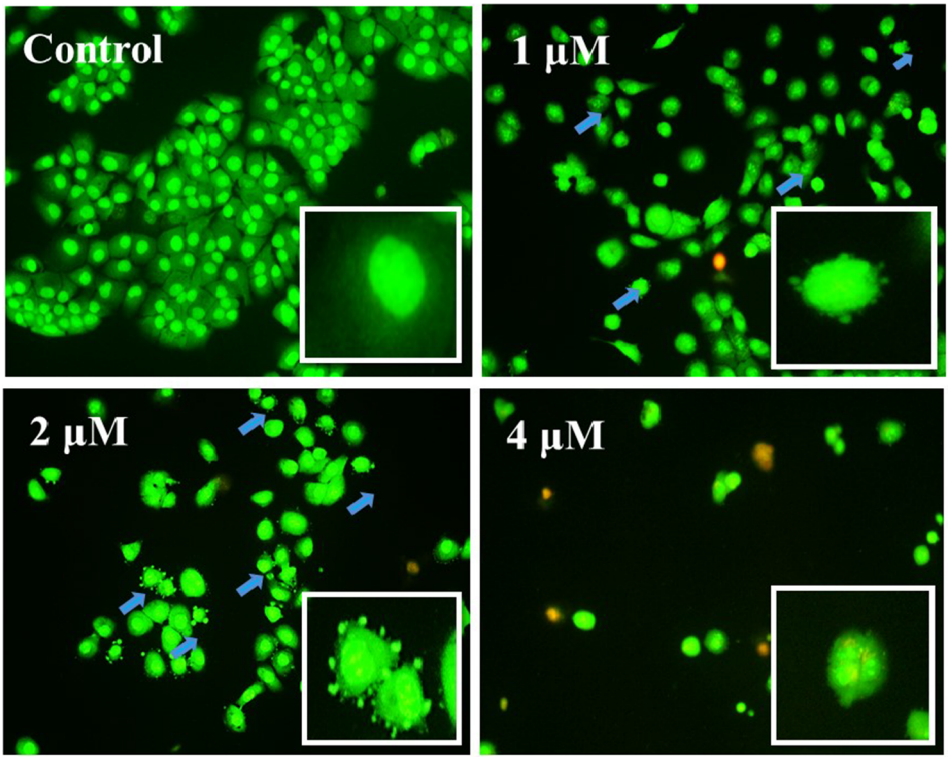

Fig. 7. Prostate cancer DU-145 cells treated with increased concentrations of compound **10e** and stained with AO/EB. Decreased number of viable cells and apoptotic characteristics (indicated by blue arrows) were observed at 200× magnification.

colony formation of cancerous cells. We believe that **10e** could be potential lead for the development of chemical library which would serves as a potential drug to treat prostate cancer.

3. Experimental section

All the starting materials, reagents and solvents used were commercially available and used directly without any further purification. TLC was performed on 0.25 mm silica gel 60-F_{254} plates. Product formation was detected by visualizing spots in UV light. All melting points were taken and are uncorrected. ^{1}H spectra were recorded on 300 and 500 MHz, ^{13}C spectra were recorded on 75, 100 and 125 MHz spectrometers using tetramethylsilane as internal standard. Chemical shifts are reported in parts per million (ppm) downfield from tetramethylsilane. Spin multiplicities are described as s (singlet), d (doublet), t (triplet), q (quartet), m (multiplet), dd (double doublet). Coupling constants are reported in hertz. HRMS analyses were acquired on single quadruple and carried out using ESI technique 70 eV. Column

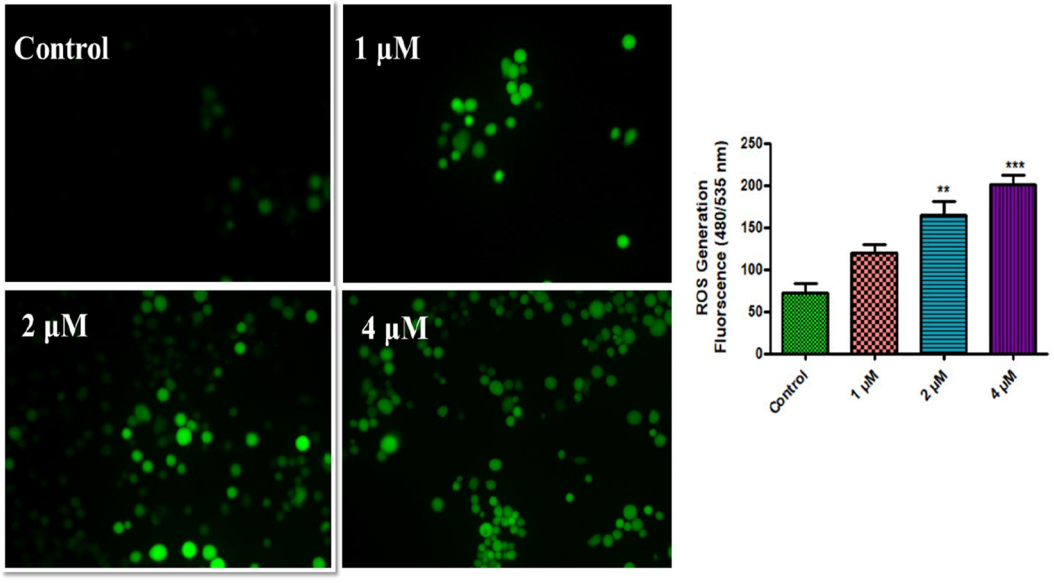

Fig. 8. DCFDA imaging depicting effect of compound 10e on generation of reactive Oxygen Species (ROS) in a.u at concentration 1, 2 and 4 μM in DU-145 prostate cancer cell lines. Graph represents the intensity of fluorescence emitted at excitation and emission wavelengths of 480 and 535 nm at various doses in comparison to control. *** < 0.001, **0.05 vs control. Data was analysed by one way ANOVA followed by Tukey's multiple comparision.

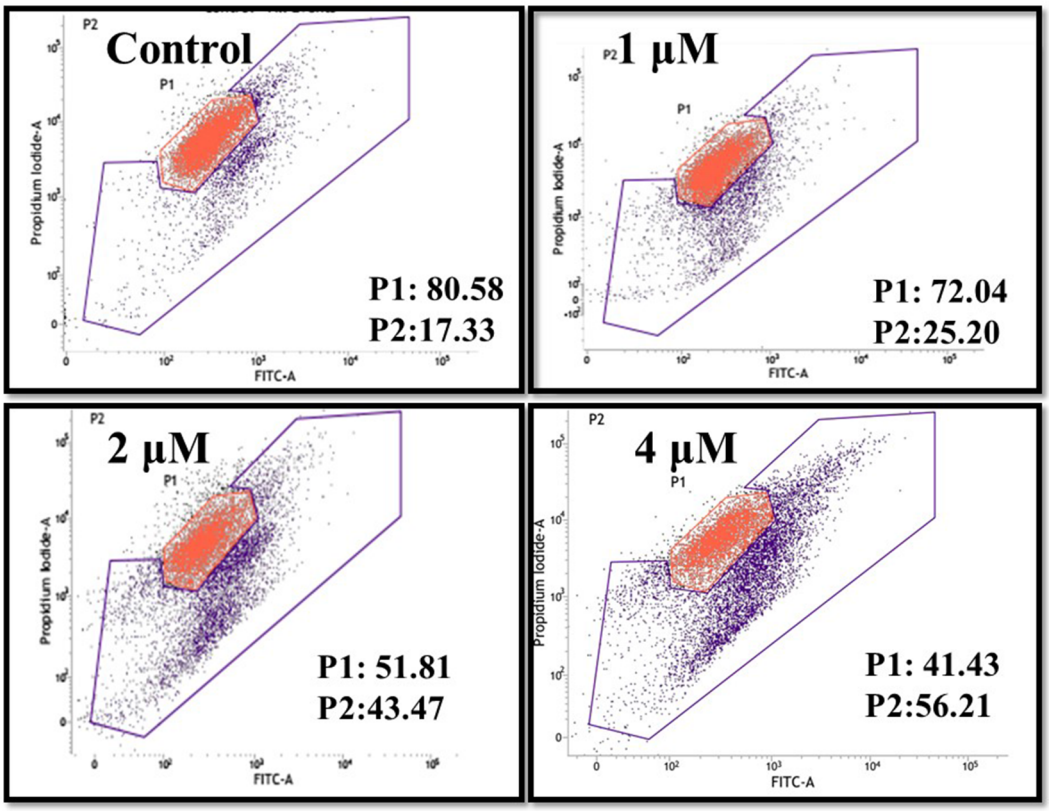

Fig. 9. Effect of compound **10e** on mitochondrial membrane potential (ΔΨm) in DU-145 prostate cancer cells upon treatment at 1, 2 and 4 μM. Cells were incubated with JC-1 dye and analysed by flow cytometer (BD FACSVerse™, USA). Values in the figures represents the J aggregates and J monomers as P1 and P2 monomers populations respectively.

chromatography was performed by using silicagel of 60–120 mm with hexane and ethyl acetate as eluents. Melting points were determined with an Electro thermal melting point apparatus and were uncorrected.

*3.1. General procedure for the preparation of substituted 2-bromo benzaldehydes (**8a-b**) [26]*

500 mL round bottom flask was charged with corresponding benzaldehydes **7a**,**b** (25.5 mmol), methylene chloride (100 mL) and acetic acid (200 mL). The RBF was cooled to 0 °C in an ice-bath and bromine (25.5 mmol) in methylene chloride (10 mL) was added drop-wise via addition funnel over 15 min. After stirring at 0 °C for half an hour, aqueous sodium thiosulfate was added and the mixture was extracted three times with CH_2Cl_2. The combined organic layers were washed with saturated aqueous sodium bicarbonate, brine and dried over sodium sulfate. Removal of the solvent under reduced pressure gave a solid, which was recrystallized (EtOAc/hexane) to give **8a**,**b** (91%) as colorless needles.

*3.2. General procedure for the preparation of substituted biphenyl 2-carbaldehydes **9a–d** [27]*

To a solution of 2-bromo-substituted benzaldehyde **8a**,**b** (1 mmol) in 3 mL ethanol, appropriate aryl boronic acid (1.1 mmol), $Pd(PPh_3)_4$ (1 mol%) sodium carbonate (1.2 mmol, dissolve in a minimum amount of water) was added. The reaction mixture was heated at 80 °C for 6 h. The solvent was removed by rotary evaporation and the product was extracted with ethyl acetate (3 × 10 mL), the organics were washed with water (2 × 10 mL), and dried over anhydrous sodium sulfate. The solvent was evaporated, and the residue was purified by column chromatography on silica gel, eluting with hexane/EtOAc mixture.

*3.3. General procedure for the synthesis of biphenyl methylene indolinones (**10a-r**)*

Oxindole (9 mmol) was added to a solution of biphenyl 2-carbaldehyde (10 mmol) in ethanol (5 mL). To that mixture catalytic amount of piperdine (1 mL) was added and the reaction mixture was allowed to stir at 80 °C for 4 h. Completion of reaction was confirmed by TLC. The solvent was removed by rotary evaporation and the product obtained was washed with methanol for 4–5 times. After complete air drying, the final compounds biphenyl methylene indolinones **10a–r** were obtained as pure solids with yield of 80%.

*3.3.1. (E)-3-((4′-Fluoro-4,5,6-trimethoxy-3′-methylbiphenyl-2-yl) methylene)indolin-2-one (**10a**)*

Yellow solid; M.p: 199–200 °C; R_f = 0.4 (40% ethyl acetate/*n*-hexane); ^{1}H NMR (500 MHz, DMSO-d_6): δ 10.52 (s, 1H), 7.60 (d, J = 7.6 Hz, 1H), 7.26–7.21 (m, 2H), 7.16 (t, J = 8.9 Hz, 2H), 7.05 (s, 1H), 7.04–6.99 (m, 1H), 6.92 (t, J = 7.6 Hz, 1H), 6.86 (d, J = 7.7 Hz, 1H), 3.88 (s, 3H), 3.82 (s, 3H), 3.59 (s, 3H), 2.26 (s, 3H). ^{13}C NMR (125 MHz, DMSO-d_6): δ 168.4, 160.06 (d, J = 243.5 Hz, 1C), 152.1, 151.1, 143.0, 142.8, 134.8, 133.3 (d, J = 5.2 Hz, 1C), 131.4 (d, J = 3.6 Hz, 1C), 129.9, 129.7 (d, J = 8.1 Hz, 1C), 128.6, 127.3, 123.6 (d, J = 17.4 Hz, 1C), 122.8, 121.1, 121.0, 114.5, 114.3, 110.1, 108.3, 60.7, 60.6, 56.2, 14.1 ppm; HRMS calculated for $[M+H]^+$ $C_{25}H_{23}FNO_4$: 420.16056 found: 420.16036.

*3.3.2. (E)-5-Chloro-3-((4′-fluoro-4,5,6-trimethoxy-3′-methylbiphenyl-2-yl)methylene)indolin-2-one (**10b**)*

Yellow solid; M.p: 234–235 °C; R_f = 0.5 (40% ethyl acetate/*n*-hexane); ^{1}H NMR (500 MHz, DMSO-d_6): δ 10.67 (s, 1H), 7.59 (s, 1H), 7.23–7.23 (m, 1H), 7.20–7.13 (m, 1H), 7.12 (s, 1H), 7.05 (s, 1H), 6.88 (d, J = 7.8 Hz, 1H) 3.89 (s, 3H), 3.84 (s, 3H), 3.59 (s, 3H), 2.25 (s, 3H)

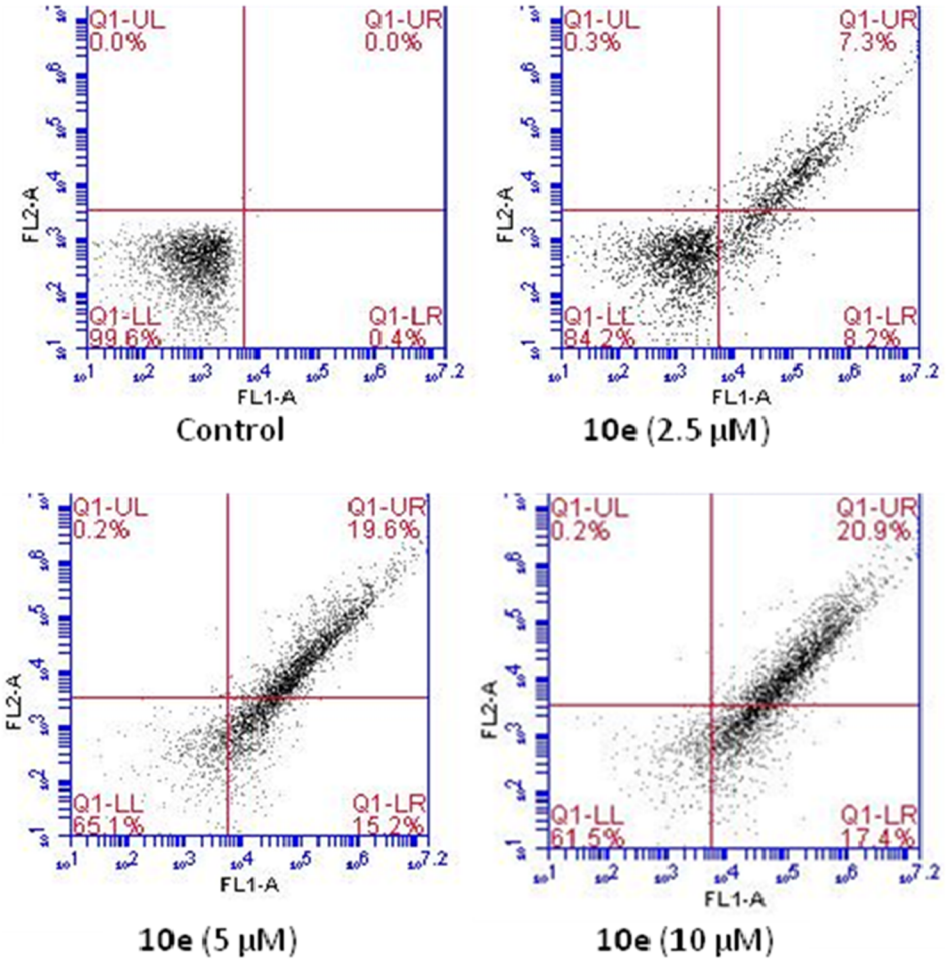

Fig. 10. Annexin V-FITC/propidium iodide dual staining assay. DU-145 cells were treated with compound **10e** and labelled with Annexin V-FITC/PI and examined for apoptosis using flow-cytometer. Cells in the lower left quadrant (Q1-LL: AV-/PI-): live cells; lower right quadrant (Q2-LR: AV-/PI-): early apoptotic cells; upper right quadrant (Q3-UR: AV + /PI +): late apoptotic cells and upper left quadrant (Q4-UL: AV − /PI +): necrotic cells.

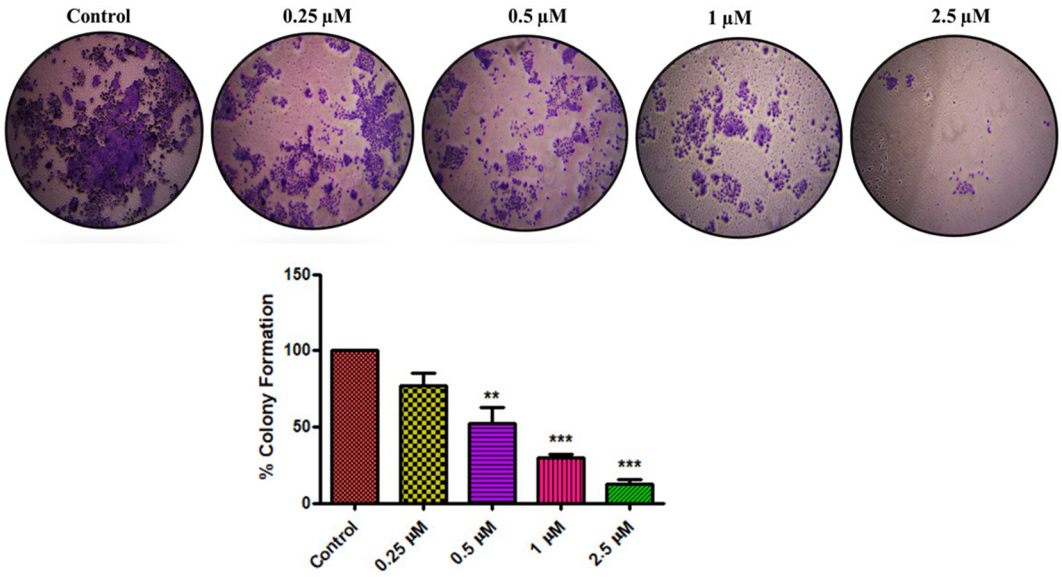

Fig. 11. Effect of compound **10e** on clonogenic assay. Control cells are having multiple colonies, while compound **10e** at concentrations of 0.25, 0.5, 1 and 2.5 µM showing inhibition of number of colonies respectively when compared to control. Images were taken at 40× magnification. Graph represents the number of average colonies represented as mean ± s.e.m of three independent experiments. *** < 0.001, ** < 0.05 vs control. Data was analysed by one way ANOVA followed by Tukey's multiple comparision.

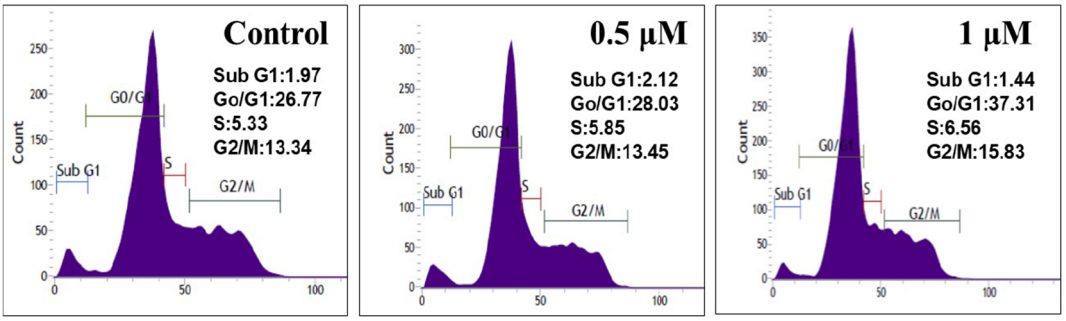

Fig. 12. Cell cycle analysis of DU-145 cells upon treatment with compound **10e** by flow cytometry. DNA histogram represents different stages of cell cycle i.e., SubG1, G0/G1, S, G2/M. Each phase of treated cells cell cycle results were compared with DMSO control cells, cell cycle analysis. 10,000 events were analysed for the results.

ppm; ^{13}C NMR (125 MHz, DMSO-d_6): δ 168.6, 160.7 (d, J = 243.7 Hz, 1C), 152.7, 151.7, 143.9, 142.1, 137.0, 133.9 (d, J = 5.1 Hz, 1C), 131.7 (d, J = 3.5 Hz, 1C), 130.3 (d, J = 8.0 Hz, 1C), 129.9, 129.6, 128.6, 126.8, 125.3, 124.2 (d, J = 17.4 Hz, 1C), 123.1, 122.9, 114.9 (d, J = 22.2 Hz, 1C), 111.9, 108.9, 61.3, 61.2, 56.1, 14.5 ppm; HRMS calculated for $[M+H]^+C_{25}H_{21}ClFNO_4$: 454.1215 found: 454.1223.

3.3.3. (E)-5-Bromo-3-((4′-fluoro-4,5,6-trimethoxy-3′-methylbiphenyl-2-yl)methylene)indolin-2-one (**10c**)

Yellow solid; M.p: 239–240 °C; R_f = 0.4 (40% ethyl acetate/*n*-hexane); ^{1}H NMR (500 MHz, DMSO-d_6): δ 10.66 (s, 1H), 7.7 (s, 1H), 4.42 (d, J = 7.8 Hz 1H), 7.28 (s, 1H), 7.21–7.12 (m, 2H), 7.11 (s, 1H), 7.05 (s, 1H), 6.84 (d, J = 7.8 Hz, 1H), 3.89 (s, 3H), 3.86 (s, 3H), 3.59 (s, 3H), 2.2 (s, 3H) ppm; ^{13}C NMR (125 MHz, DMSO-d_6): δ 168.4, 161.5 (d, J = 243.7 Hz, 1C), 152.7, 151.7, 143.9, 142.4, 137.0, 133.9, 132.6, 131.7, 130.4, 130.3, 128.5, 126.6, 125.7, 124.3 (d, J = 17.5 Hz, 1C), 123.7, 114.9 (d, J = 22.1 Hz, 1C), 112.9, 112.5, 108.8, 61.3, 61.2, 56.5, 14.2 ppm; HRMS calculated for $[M]^+C_{25}H_{21}BrFNO_4$: 497.0638 found: 497.0635.

3.3.4. (E)-5-Fluoro-3-((4′-fluoro-4,5,6-trimethoxy-3′-methylbiphenyl-2-yl)methylene)indolin-2-one (**10d**)

Yellow solid; M.p: 233–234 °C; R_f = 0.4 (50% ethyl acetate/*n*-hexane); ^{1}H NMR (500 MHz, DMSO-d_6): δ 10.55 (s, 1H), 7.30 (dd, J = 9.2, 2.2 Hz, 1H), 7.23 (s, 1H), 7.16 (t, J = 9.0 Hz, 2H), 7.12 (s, 1H), 7.09 (dd, J = 9.0, 2.4 Hz, 1H), 7.05–7.00 (m, 1H), 6.86 (dd, J = 8.5, 4.6 Hz, 1H), 3.89 (m, 3H), 3.83 (s, 3H), 3.60 (s, 3H), 2.25 (s, 3H) ppm; ^{13}C NMR (125 MHz, DMSO-d_6): δ 168.8, 160.6 (d, J = 243.6 Hz, 1C), 157.67 (d, J = 235.2 Hz, 1C), 152.8, 151.7, 143.7, 139.7, 137.0, 133.9, 131.7, 130.2, 129.3, 128.7, 127.4, 124.2 (d, J = 17.4, Hz, 1C), 122.57 (d, J = 8.9 Hz, 1C), 116.7 (d, J = 23.6 Hz, 1C), 115.0 (d, J = 22.2 Hz, 1C), 113.0 (d, J = 8.3 Hz, 1C), 111.3 (d, J = 8.3 Hz, 1C), 110.2 (d, J = 25.9 Hz, 1C), 108.7, 61.3, 61.1, 56.6, 14.6 ppm; HRMS calculated for $[M+H]^+C_{25}H_{21}F_2NO_4$: 438.1517 found: 438.1513.

3.3.5. (E)-6-chloro-3-((4′-fluoro-4,5,6-trimethoxy-3′-methylbiphenyl-2-yl) methylene)indolin-2-one (**10e**)

Yellow solid; M.p: 240–241 °C; R_f = 0.4 (30% ethyl acetate/*n*-hexane); ^{1}H NMR (500 MHz, DMSO-d_6): δ 10.69 (s, 1H), 7.60 (d, J = 8.3 Hz, 1H), 7.21 (s, 1H), 7.19–7.11 (m, 2H), 7.07 (s, 1H), 7.05 – 6.97 (m, 2H), 6.88 (d, J = 1.7 Hz, 1H), 3.88 (s, 3H), 3.82 (s, 3H), 3.58 (s, 3H), 2.25 (s, 3H) ppm; ^{13}C NMR (125 MHz, DMSO-d_6): δ 168.3, 161.0 (d, J = 243.6 Hz, 1C), 152.3, 151.1, 144.1, 143.3, 135.6, 133.9, 133.4, 131.3, 129.7 (d, J = 8.2 Hz 1C), 128.7, 128.3, 126.1, 124.1, 123.7, 123.6, 120.9, 119.9, 114.4 (d, J = 22.2 Hz), 110.0, 108.2, 60.7, 60.6, 56.0, 14.1 ppm; HRMS calculated for $[M+H]^+$ $C_{25}H_{21}ClFNO_4$: 454.1215 found: 454.1223.

3.3.6. (E)-3-((3′-Fluoro-4,5,6-trimethoxybiphenyl-2-yl)methylene)indolin-2-one (**10f**)

Yellow solid; M.p: 193–194 °C; R_f = 0.4 (40% ethyl acetate/*n*-hexane); ^{1}H NMR (300 MHz, $CDCl_3$): δ 8.62 (s, 1H), 7.67 (d, J = 7.5 Hz, 1H), 7.36–7.20 (m, 4H), 7.08–6.99 (m, 3H), 6.94–6.88 (m, 2H), 4.01 (s, 3H), 3.86 (s, 3H), 3.68 (s, 3H) ppm; ^{13}C NMR (125 MHz, $CDCl_3$): δ 169.9, 163.2 (d, J = 246.1 Hz, 1C), 152.6, 151.5, 143.6, 141.8, 137.4, 137.0, 129.8, 129.4, 129.1, 128.9, 127.4, 126.6, 123.0, 121.7, 121.5,

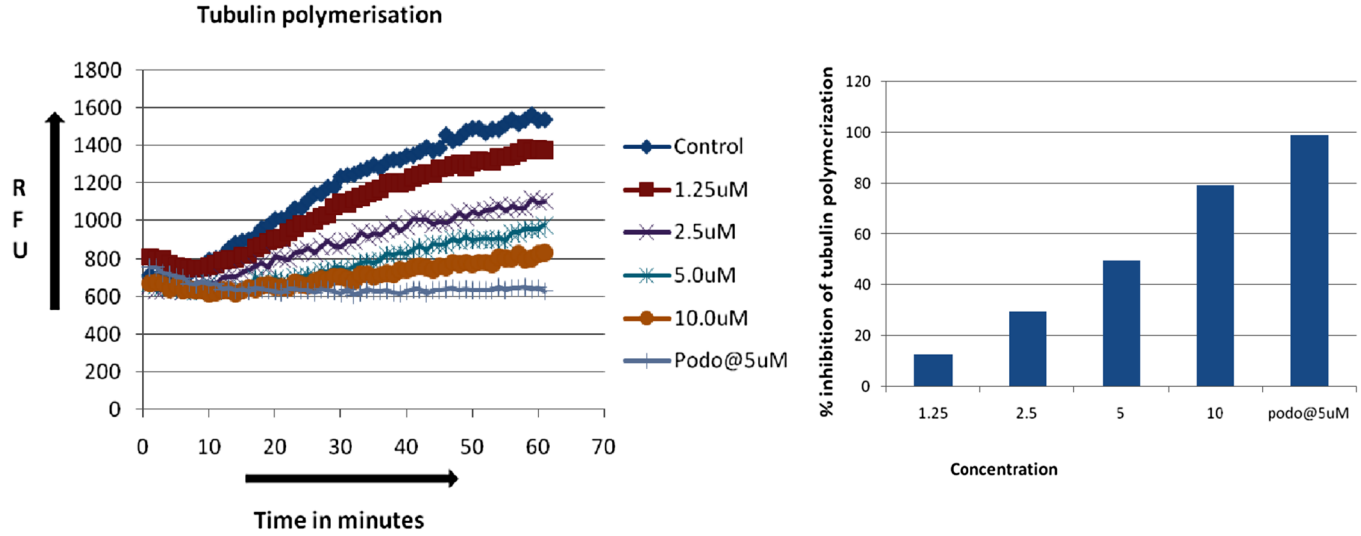

Fig. 13. Effect of compound **10e** on tubulin polymerization inhibition.

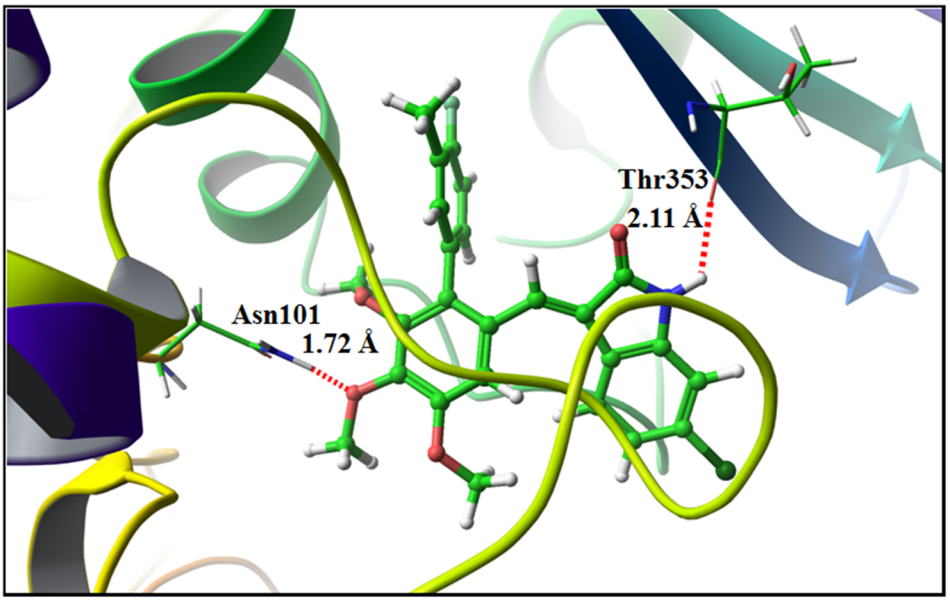

Fig. 14. Docking pose of the most potent compound **10e** (green colour ball and stick) in the colchicine binding site of α/β-tubulin interface and the interacting amino acids (PDB ID: 3E22). The red dashed lines represent hydrogen bonds.

117.6 (d, J = 21.8 Hz, 1C), 114.7 (d, J = 20.9 Hz, 1C), 110.4, 108.3, 61.1, 61.0, 56.1 ppm; HRMS calculated for $[M+H]^+C_{24}H_{20}FNO_4$: 406.1455 found: 406.1449.

3.3.7. *(E)-5-Chloro-3-((3′-fluoro-4,5,6-trimethoxybiphenyl-2-yl) methylene)indolin-2-one (**10g**)*

Yellow solid; M.p: 231–232 °C; R_f = 0.5 (40% ethyl acetate/*n*-hexane); ^{1}H NMR (500 MHz, $CDCl_3$): δ 8.49 (s, 1H), 7.75 (s, 1H), 7.38 (s, 1H), 7.36–7.32 (m, 1H), 7.20 (d, J = 7.9 Hz, 1H), 7.16 (s, 1H), 7.08–6.99 (m, 3H), 6.82 (d, J = 8.2 Hz, 1H), 4.02 (s, 3H), 3.90 (s, 3H), 3.67 (s, 3H) ppm; ^{13}C NMR (125 MHz, DMSO-d_6): δ 168.5, 161.9 (d, J = 243.7 Hz, 1C), 153.1, 151.7, 143.9, 142.1, 138.2, 136.8, 130.3, 129.9, 128.9, 128.6, 127.2, 127.1, 125.3, 123.1, 123.0, 117.6 (d, J = 21.2 Hz, 1C), 114.9 (d, J = 20.7 Hz, 1C), 111.9, 108.9, 61.3, 61.2, 56.5 ppm; HRMS calculated for $[M+H]^+C_{24}H_{19}ClFNO_4$: 440.0987 found: 440.1068.

3.3.8. *(E)-6-Chloro-3-((3′-fluoro-4,5,6-trimethoxybiphenyl-2-yl) methylene)indolin-2-one (**10h**)*

Yellow solid; M.p: 219–220 °C; R_f = 0.5 (40% ethyl acetate/*n*-hexane); ^{1}H NMR (500 MHz, $CDCl_3$): δ 8.39 (s, 1H), 7.58 (d, J = 8.2 Hz, 1H), 7.35 (s, 1H), 7.34–7.30 (m, 1H), 7.10 (s, 1H), 7.07–7.02 (m, 1H), 7.01–6.97 (m, 2H), 6.91–6.87 (m, 2H), 4.01 (s, 3H), 3.85 (s, 3H), 3.66 (s, 3H); ^{13}C NMR (75 MHz, $CDCl_3$ + DMSO-d_6): δ 168.5, 163.0 (d, J = 245.9 Hz, 1C), 152.0, 150.7, 143.4, 142.7, 137.0, 135.4, 134.2, 128.7, 128.2, 128.0, 126.2, 125.9, 122.9, 120.1, 119.4, 116.8 (d, J = 21.4 Hz, 1C), 113.8 (d, J = 20.9 Hz, 1C), 110.0, 107.4, 60.3, 60.2, 55.4 ppm; HRMS calculated for $[M+H]^+C_{24}H_{19}ClFNO_4$: 440.0987 found: 440.1068.

3.3.9. *(E)-5-Fluoro-3-((3′-fluoro-4,5,6-trimethoxybiphenyl-2-yl) methylene)indolin-2-one (**10i**)*

Yellow solid; M.p: 225–226 °C; R_f = 0.4 (50% ethyl acetate/*n*-hexane); ^{1}H NMR (500 MHz, $CDCl_3$): δ 8.48 (s, 1H), 7.75 (s, 1H), 7.39–7.30 (m, 2H), 7.22–7.15 (m, 2H), 7.08–6.99 (m, 3H), 6.82 (d,

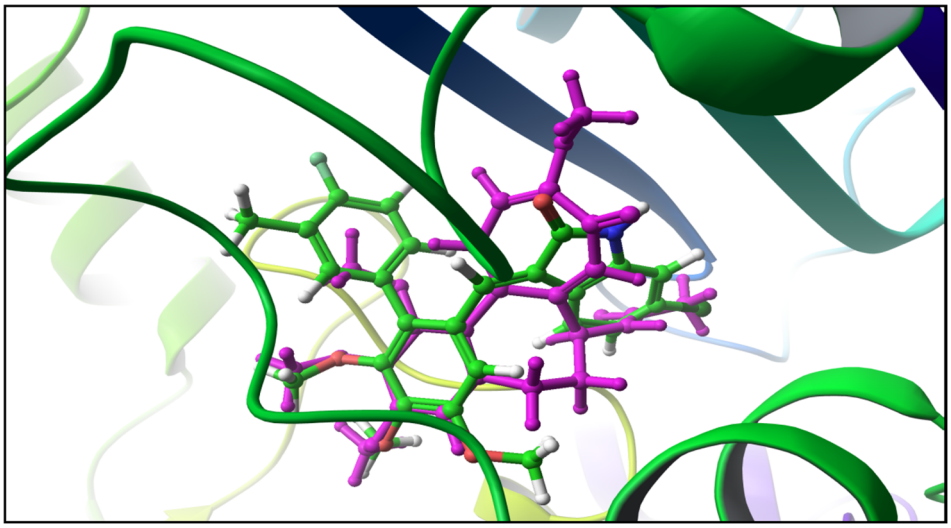

Fig. 15. Superimposition of co-crystallized ligand (magenta) and the best docked pose of compound **10e** (green) in the colchicine binding site of α/β-tubulin interface (PDB ID: 3E22).

J = 8.2 Hz, 1H), 4.03 (s, 3H), 3.89 (s, 3H), 3.68 (s, 3H) ppm; ^{13}C NMR (125 MHz, DMSO-d_6): δ 168.8, 161.6 (d, J = 245.9 Hz, 1C), 158.6 (d, J = 235.9 Hz, 1C), 152.8, 151.7, 143.8, 139.6, 137.0, 133.9, 131.8, 130.2, 129.3, 128.7, 127.5, 124.3, 122.6, 116.8, 111.3, 110.1, 108.7, 61.3, 61.1, 56.6 ppm; HRMS calculated for $[M+H]^+C_{24}H_{19}F_2NO_4$: 424.1360 found: 424.1364.

*3.3.10. (E)-5-Bromo-3-((3′-fluoro-4,5,6-trimethoxybiphenyl-2-yl) methylene)indolin-2-one (**10j**)*

Yellow solid; M.p: 237–238 °C; R_f = 0.4 (40% ethyl acetate/*n*-hexane); ^{1}H NMR (500 MHz, $CDCl_3$): δ 8.49 (s, 1H), 7.38–7.32 (m, 3H), 7.17 (s, 1H), 7.08–6.99 (m, 3H), 6.78 (d, J = 7.6 Hz, 1H), 4.02 (s, 3H), 3.91 (s, 3H), 3.67 (s, 3H) ppm; ^{13}C NMR (100 MHz, $CDCl_3$): δ 169.6, 162.4 (d, J = 245.7 Hz, 1C), 152.7, 151.7, 1441.2, 140.6, 138.7, 137.3, 132.1, 129.6, 129.4, 129.3, 128.2, 126.7, 125.9, 123.5, 117.6 (d, J = 22.0, 1C), 114.8 (d, J = 21.3, 1C), 114.1, 111.8, 108.1, 61.8, 61.0, 56.2 ppm; HRMS calculated for $[M+H]^+C_{24}H_{19}BrFNO_4$: 484.0560 found: 480.0561.

*3.3.11. (E)-3-((4′-Fluoro-4,5-dimethoxy-3′-methylbiphenyl-2-yl) methylene)indolin-2-one (**10k**)*

Yellow solid; M.p: 228–229 °C; R_f = 0.5 (40% ethyl acetate/*n*-hexane); ^{1}H NMR (500 MHz, DMSO-d_6): δ 10.51 (s, 1H), 7.64 (d, J = 7.6 Hz, 1H), 7.38 (s, 1H), 7.32 (d, J = 6.1 Hz, 1H), 7.26 (s, 1H), 7.24–7.20 (m, 1H), 7.18 (d, J = 9.3 Hz, 1H), 7.17–7.11 (m, 1H), 7.08 (s, 1H), 6.95–6.86 (m, 2H), 3.91 (s, 3H), 3.79 (s, 3H), 2.27 (s, 3H) ppm; ^{13}C NMR (75 MHz, $CDCl_3$): δ 168.1, 159.2 (d, J = 244.8 Hz, 1C), 148.8, 146.4, 141.4, 134.9, 134.2, 131.3, 128.2, 127.7, 127.6, 125.3, 123.4, 123.2 (d, J = 18.1 Hz, 1C), 121.3, 120.3, 119.6 (d, J = 11.5 Hz, 1C), 113.5 (d, J = 22.5 Hz, 1C), 111.6, 110.9, 109.1, 54.7, 54.6, 13.1 ppm; HRMS calculated for $[M+H]^+C_{24}H_{20}FNO_3$: 390.1500 found: 390.1509.

*3.3.12. (E)-5-Chloro-3-((4′-fluoro-4,5-dimethoxy-3′-methylbiphenyl-2-yl) methylene)indolin-2-one (**10l**)*

Yellow solid; M.p: 290–291 °C; R_f = 0.6 (40% ethyl acetate/*n*-hexane); ^{1}H NMR (500 MHz, DMSO-d_6): δ 10.66 (s, 1H), 7.62 (s, 2H), 7.44–7.22 (m, 4H), 7.23–7.06 (m, 3H), 6.90 (s, 1H), 3.92 (s, 3H), 3.81 (s, 3H), 2.28 (s, 3H) ppm; ^{13}C NMR (125 MHz, DMSO-d_6): δ 168.9, 159.8 (d, J = 234.5 Hz, 1C), 151.1, 148.3, 141.9, 137.6, 135.8, 133.1, 129.7, 129.6, 129.5, 125.80, 125.2, 124.7 (d, J = 17.3 Hz, 1C), 124.1, 123.5, 122.7, 115.2 (d, J = 22.6 Hz, 1C), 113.9, 112.7, 111.8, 56.3, 56.2, 14.5 ppm; HRMS calculated for $[M+H]^+C_{24}H_{19}ClFNO_3$: 424.1110 found: 424.1118.

*3.3.13. (E)-6-Chloro-3-((4′-fluoro-4,5-dimethoxy-3′-methylbiphenyl-2-yl) methylene)indolin-2-one (**10m**)*

Yellow solid; M.p: 295–296 °C; R_f = 0.6 (40% ethyl acetate/*n*-hexane); ^{1}H NMR (500 MHz, DMSO-d_6): δ 10.67 (s, 1H), 7.64 (s, 1H), 7.42 – 7.25 (m, 3H), 7.25–7.11 (m, 2H), 7.09 (s, 1H), 7.02–6.99 (m, 1H), 6.90 (s, 1H), 3.91 (s, 3H), 3.79 (s, 3H), 2.27 (s, 3H) ppm; ^{13}C NMR (125 MHz, DMSO-d_6): δ 169.1, 160.8 (d, J = 237.5 Hz, 1C), 150.8, 148.3, 144.5, 136.7, 136.0, 135.6, 134.1, 133.2, 129.6, 125.7, 124.8, 124.6, 124.3, 121.3, 120.7, 115.1, 113.7, 112.5, 110.4, 56.3, 56.2, 14.6 ppm; HRMS calculated for $[M+H]^+C_{24}H_{19}ClFNO_3$: 424.1110 found: 424.1118.

*3.3.14. (E)-5-Bromo-3-((4′-fluoro-4,5-dimethoxy-3′-methylbiphenyl-2-yl) methylene)indolin-2-one (**10n**)*

Yellow solid; M.p: 285–286 °C; R_f = 0.5 (40% ethyl acetate/*n*-hexane); ^{1}H NMR (500 MHz, DMSO-d_6): δ 10.67 (s, 1H), 7.78 (s, 1H), 7.47–7.38 (m, 2H), 7.34 (d, J = 6.8 Hz, 1H), 7.31 (s, 1H), 7.23–7.14 (m, 2H), 7.11 (s, 1H), 6.86 (d, J = 8.2 Hz, 1H), 3.92 (s, 3H), 3.82 (s, 3H), 2.28 (s, 3H) ppm; ^{13}C NMR (125 MHz, DMSO-d_6): δ 168.7, 160.40, 150.9, 148.1, 142.23, 137.6, 135.9, 135.8, 133.2, 132.2, 129.7, 125.60, 125.4, 124.8, 124.6, 124.1, 115.2, 113.9, 112.9, 112.6, 112.3, 56.3, 56.2, 14.6 ppm; HRMS calculated for $[M+H]^+C_{24}H_{19}BrFNO_3$: 468.0605 found: 468.0616.

*3.3.15. (E)-3-((3′-Fluoro-4,5-dimethoxybiphenyl-2-yl)methylene)indolin-2-one (**10o**)*

Yellow solid; M.p: 233–234 °C; R_f = 0.6 (40% ethyl acetate/*n*-hexane); ^{1}H NMR (500 MHz, $CDCl_3$): δ 8.29 (s, 1H), 7.71 (d, J = 7.6 Hz, 1H), 7.56 (s, 1H), 7.38 (s, 1H), 7.35 (q, J = 7.9, 14.0 Hz, 1H), 7.23 (t, J = 7.8 Hz, 1H), 7.12 (d, J = 7.6 Hz, 1H), 7.09–7.03 (m, 2H), 6.98 (s, 1H), 6.93–6.89 (m, 2H), 4.00 (s, 3H), 3.88 (s, 3H) ppm; ^{13}C NMR (125 MHz, $CDCl_3$): δ 170.1, 162.3 (d, J = 247.0 Hz, 1C), 150.3, 148.1, 141.9, 141.6, 137.5, 135.2, 129.8 (d, J = 8.2 Hz, 1C), 129.6, 126.7, 125.7, 125.0, 122.9, 121.9, 121.5, 116.5 (d, J = 21.8 Hz, 1C), 114.5 (d, J = 20.8 Hz, 1C), 112.7, 112.2, 110.4, 56.2, 56.0 ppm; HRMS calculated for $[M+H]^+C_{23}H_{19}FNO_3$: 376.1343 found: 376.1351.

*3.3.16. (E)-5-Chloro-3-((3′-fluoro-4,5-dimethoxybiphenyl-2-yl) methylene)indolin-2-one (**10p**)*

Yellow solid; M.p: 275–276 °C; R_f = 0.5 (30% ethyl acetate/*n*-hexane); ^{1}H NMR (500 MHz, DMSO-d_6): δ 10.69 (s, 1H), 7.59 (s, 1H), 7.53–7.44 (m, 1H), 7.42 (s, 1H), 7.34 (s, 1H), 7.29–7.20 (m, 3H), 7.19–7.13 (m, 2H), 6.90 (d, J = 7.1 Hz, 1H), 3.93 (s, 2H), 3.82 (s, 1H) ppm; ^{13}C NMR (125 MHz, DMSO-d_6): δ 168.8, 162.2 (d, J = 242.3 Hz, 1C), 151.0, 148.6, 142.2, 142.0, 137.3, 135.2, 130.7 (d, J = 8.4 Hz, 1C), 129.6, 126.5, 126.2, 125.3, 124.2, 123.4, 122.7, 116.8 (d, J = 21.8 Hz, 1C), 114.8 (d, J = 20.9 Hz, 1C), 113.9, 112.7, 111.8, 56.3, 56.3 ppm; HRMS calculated for $[M+H]^+C_{23}H_{18}$ $ClFNO_3$: 410.0959 found: 410.1121.

*3.3.17. (E)-5-Fluoro-3-((3′-fluoro-4,5-dimethoxybiphenyl-2-yl)methylene) indolin-2-one (**10q**)*

Yellow solid; M.p: 218–219 °C; R_f = 0.4 (40% ethyl acetate/*n*-hexane); ^{1}H NMR (500 MHz, DMSO-d_6): δ 10.57 (s, 1H), 8.44 (s, 1H), 7.50–7.43 (m, 1H), 7.37 (d, J = 8.6 Hz, 1H), 7.27–7.21 (m, 2H), 7.20–7.14 (m, 2H), 7.12–7.06 (m, 1H), 6.89–6.83 (m, 1H), 3.93 (s, 1H), 3.81 (s, 2H) ppm; ^{13}C NMR (125 MHz, DMSO-d_6): δ 169.0, 149.9 (d, J = 227.4 Hz, 1C), 149.7 (d, J = 245.3 Hz, 1C), 142.3, 139.5, 139.90, 137.3, 134.9, 130.7, 127.0, 126.5, 124.3, 123.5, 116.8, 116.6, 114.7, 113.9, 112.6, 111.2, 110.2, 109.9, 56.1 ppm; HRMS calculated for $[M+H]^+C_{23}H_{18}$ F_2NO_3: 394.1255 found: 394.1250.

*3.3.18. (E)-6-Chloro-3-((3′-fluoro-4,5-dimethoxybiphenyl-2-yl) methylene)indolin-2-one (**10r**)*

Yellow solid; M.p: 278–279 °C; R_f = 0.5 (30% ethyl acetate/*n*-hexane); ^{1}H NMR (500 MHz, DMSO-d_6): δ 10.70 (s, 1H), 7.60 (d, J = 8.2 Hz, 1H), 7.47 (dd, J = 14.1, 7.2 Hz, 1H), 7.36 (s, 1H), 7.32 (s, 1H), 7.24 (t, J = 8.7 Hz, 2H), 7.17 (d, J = 7.6 Hz, 1H), 7.14 (s, 1H), 6.98 (d, J = 7.4 Hz, 1H), 6.90 (s, 1H), 3.92 (s, 3H), 3.80 (s, 3H) ppm; ^{13}C NMR (125 MHz, DMSO-d_6): δ 169.0, 162.4 (d, J = 244.2 Hz, 1C), 150.8, 148.7, 144.5, 142.3 (d, J = 8.0 Hz, 1C), 136.4, 134.9, 134.2, 130.7, 126.5, 126.1, 124.5 (d, J = 7.3 Hz, 1C), 121.4, 120.7, 116.8, 114.8 (d, J = 20.8 Hz, 1C), 113.8, 112.6, 110.4, 56.3, 56.2 ppm; HRMS calculated for $[M+H]^+C_{23}H_{18}$ $ClFNO_3$: 410.0959 found: 410.1121.

4. Biology

4.1. Material and methods

Prostate cancer (DU-145) mouse breast cancer cell line (4T1), human breast cancer cell line (MDA-MB-231), human urinary bladder carcinoma cell line (T24), cervical cancer cell lines (HeLa) were obtained from National center for cell Science (NCCS, Pune). Cells were cultured in respective RPMI (Roswell Park Memorial Institute medium, Sigma Aldrich, St. Louis, USA) and Dulbecco's Modified Eagle's medium (DMEM), supplemented with 10% fetal bovine serum (FBS) (Gibco, USA) and 1% stabilized antibiotic, penicillin-streptomycin mixture (Gibco, USA). Cells were maintained in a CO_2 incubator at 37 °C with

5% CO_2 and 90% relative humidity. Trypsin-EDTA required for cell culture was obtained from (Gibco, USA). Fluorescent dyes acridine orange (AO), 4′, 6-diamidino-2-phenylindole (DAPI) were from Sigma Aldrich, St. Louis, USA, and Ethidium Bromide (EB) from Himedia limited India, while Dichlorofluorescin diacetate (DCFDA) and JC-1 dyes were procured from Invitrogen, USA.

4.1.1. Cytotoxic activity

Cytotoxic activity of compounds of the series **10a-r** was carried out by MTT assay. Cells were plated at a density of 5×10^3 cells per well in a 96 well plate supplemented with 10% FBS and after 24 h of incubation at 37 °C in 5% CO_2 they were treated with respective concentration of the compounds dissolved in the culture media with vehicle controls and known standards. The test compounds were initially dissolved in DMSO and made up the required concentration with media. Then after 48 h of treatment, 100 µL MTT (3-(4,5-dimethylthiazol-2-yl)-2,5-diphenyl tetrazolium bromide) reagent (0.5 mg/mL) dissolved in serum free media was added to each well and incubated for 4 h. Then the media was aspirated and the formazan crystals were dissolved in 200 µL of DMSO and absorbance was taken at 570 nm in multimode plate reader (Spectra Max M4, Molecular devices, US).

4.1.2. Cell morphology by phase contrast imaging

DU-145 cells were plated with density of 1×10^5 cells/mL in 6 well culture plates and allowed to adhere for overnight by incubating at 37 °C in an atmosphere of 5% CO_2 for 48 h. Cells were incubated with various concentrations of compound **10e** (1, 2 and 4 µM). Morphological changes and viability were studied after 48 h of incubation with compound **10e**, and respective images were captured by using phase contrast microscope (Nikon, Inc. Japan).

4.1.3. DAPI staining

Compound **10e** induced morphological changes in the nucleus were studied using DAPI staining [28]. Here cells were seeded at density of 2×10^5 cells/well and allowed to adhere for overnight. Next day cells were incubated with compound **10e** for 48 h. After incubation cells were washed with PBS and solubilized with 0.1% Tween 20 for 5 min after fixing with 4% *para* formaldehyde followed by staining with 1 mM DAPI. Control and treated cells were observed with fluorescence microscope with wavelengths of excitation at 359 nm and emission at 461 nm using DAPI filter in fluorescent microscope at 200 magnifications and representative images were captured.

4.1.4. Acridine orange (AO) and ethyl bromide (EB) staining

DU-145 cells were plated with density of 2×10^5 cells/mL. Upon adhering for overnight, cells were incubated after treatment with different concentrations of compound **10e** (1, 2 and 4 µM) and maintained at 37 °C in an atmosphere of 5% CO_2 for 48 h. For AO/EB staining, both the dyes of 1 mg/mL concentration were taken and added into wells reach concentration of 10 µg/mL. After 10 min of incubation, the cells were visualized under fluorescence microscope (Nikon, Inc. Japan) with wavelengths of excitation 488 nm and emission 550 nm at 200 magnifications and representative images were captured.

4.1.5. Measurement of reactive oxygen species (ROS) generation by DCFDA staining

DU-145 cells with a density of 2×10^5 cells/mL were plated in 6 well plates and allowed to adhere for overnight. Later the cells were treated with concentration 1, 2 and 4 µM of compound **10e** for 48 h. The media was replaced with culture medium containing DCFDA dye (10 mM) and incubated in dark for 30 min. The intensity of this fluorescence from cells was determined by florescence spectroscopy (SpectraMax, Molecular devices) at an excitation and emission wavelength of 480 and 535 nm respectively and the corresponding images were captured by fluorescent microscope.

4.1.6. Measurement of mitochondrial membrane potential by JC-1 staining

DU-145 cells were cultured in 6 well plates at a density of 5×10^5 cells/mL and allowed to grow over night. After adhering, cells were treated with 1, 2, and 4 µM concentrations of the compound **10e**. After 48 h of incubation, cells were incubated with JC-1 stain [29] (2.5 mg/mL) later adhered cells were collected by trypsinsation, washed with PBS and resuspended in a solution of PBS. The samples were then analysed for JC-1 fluorescence using flow-cytometer (BD FACSVerseTM, USA).

4.1.7. Clonogenic assay

Prostate cancer DU-145 cells were plated at a density of 250 cells/well and left to adhere for overnight. After adhering, cells were exposed to compound **10e** at doses of 0.25, 0.5, 1 and 2.5 µM for 24 hr. Post to incubation, treatment was washed with media, cells were maintained in complete media and allowed to grow them as colonies for 10 days. Cells were observed for colonies during this period. After 10 days colonies which were formed were stained with 1% crystal violet stain for 4 h. The colonies with cells greater than 25 were considered and counted under phase contrast microscope and representative images were captured. (Colony formations were calculated as percentage to control cells).

4.1.8. Annexin V binding assay

In order to determine the apoptosis induced cell death annexin V FITC and propidium iodide staining was performed by using the Annexin V FITC apoptosis detection kit according to manufacturer's protocol (Sigma Aldrich). In brief, cells were seeded at a density of 1×10^6 cells per well in a 6 well plate and allowed to adhere for overnight. The cells were treated with different concentrations of 2.5 µM, 5 µM and 10 µM compounds along with the control. After 24 h of incubation, the cells were harvested, washed with PBS and stained with Annexin V FITC and propidium iodide. Early and late apoptotic cells were quantified using Accuri C6 flow cytometer based software (BD Biosciences).

4.1.9. Flow cytometry based for cell cycle analysis

DU-145 cells were seeded with the density of 1×10^6/well in six well plate for 24 h. After 24 h, cells were subjected to starvation (serum free) for 6 h followed by treatment with 0.5 and 1 µM concentrations of compound **10e** in 5% complete medium for 24 h, later adhered cells were collected by trypsinisation, washed twice with PBS (pH 7.4) and fixed with 70% ice cold ethanol for overnight at −20 °C. Following fixation cells were rewashed twice with PBS and stained with (450 µL) propidium Iodide (PI) staining buffer for 15 mins in dark at room temperature (5). The stained samples were then analysed for PI fluorescence by flow cytometry (BD FACSVerseTM, USA). 10,000 events were considered for analysing results.

4.1.10. Tubulin polymerization assay

To evaluate the effect of **10e** on tubulin polymerization, fluorescence based *in vitro* tubulin polymerization assay was performed according to the manufacturer's protocol (BK011, Cytoskeleton, Inc.). The reaction mixture for the experiment is having Porcine brain tissue (2 mg/mL) in 80 mM PIPES pH 6.9, 2.0 mM $MgCl_2$, 0.5 mM EGTA, 1.0 mM GTP and glycerol in the presence or absence of test compound **10e** (final concentration of 10, 5, 2.5, 1.25 µM). Podophyllotoxin was used as standard in this assay at 5 µM final concentration. Polymerization was monitored by increase in the fluorescence at 37 °C. Tubulin polymerization was followed by a time dependent increase in fluorescence due to the incorporation of a fluorescence reporter into microtubules as polymerization proceeds. Fluorescence emission at 440 nm (excitation wavelength is 360 nm) was measured by using a spectramax M4 multi mode micro plate detection System. The IC_{50} value was calculated from the compound concentration required to inhibit 50% of tubulin assembly in comparison to control.

4.1.11. Molecular docking simulation study

The 3D structure of compound **10e** was built on Maestro Molecule Builder of Schrödinger. The built molecule was optimized using OPLS_2005 force field in Lig Prep module of Schrödinger software. Docking procedure was followed using the standard protocol implemented in Maestro, version 9.9 and the compound **10e** was docked against the colchicine binding site of α/β-tubulin interphase. The ligand–protein complex was analysed for interactions and the 3D pose of most active compound **10e** was taken using Schrödinger.

Acknowledgements

The authors are thankful to DoP, Ministry of Chemicals & Fertilizers, Govt. of India, for the award of NIPER fellowship. Dr. N. Shankaraiah gratefully acknowledge to SERB, DST, Govt. of India for research grant (YSS-2015-001709).

Appendix A. Supplementary material

Supplementary data to this article can be found online at https://doi.org/10.1016/j.bioorg.2019.01.063.

References

[1] Y. Lu, J. Chen, M. Xiao, W. Li, D.D. Miller, An overview of tubulin inhibitors that interact with the colchicine binding site, Pharm. Res. 29 (2012) 2943–2971.
[2] C. Dumontet, M.A. Jordan, Microtubule-binding agents: a dynamic field of cancer therapeutics, Nat. Rev. Drug Discov. 9 (2010) 790–803.
[3] M.A. Jordan, L. Wilson, Microtubules as a target for anti-cancer drugs, Nat. Rev. Cancer. 4 (2004) 253–26.
[4] B. Pandit, Y. Sun, P. Chen, D.L. Sackett, Z. Hu, W. Rich, C. Li, A. Lewis, K. Schaefer, P.K. Li, Structure–activity-relationship studies of conformationally restricted analogs of combretastatin A-4 derived from SU5416, Bioorg. Med. Chem. 14 (2006) 6492–6501.
[5] (a) Y. Lu, J. Chen, M. Xiao, W. Li, D.D. Miller, An overview of tubulin inhibitors that interact with the colchicine binding site, Pharm. Res. 29 (2012) 2943–2971; (b) A.S. Kumar, M.A. Reddy, N. Jain, C. Kishor, T.R. Murthy, D. Ramesh, B. Supriya, A. Addlagatta, S.V. Kalivendi, B. Sreedhar, Design and synthesis of biaryl aryl stilbenes/ethylenes as antimicrotubule agents, Eur. J. Med. Chem. 60 (2013) 305–324.
[6] A. Andreani, S. Burnelli, M. Granaiola, A. Leoni, A. Locatelli, R. Morigi, M. Rambaldi, L. Varoli, M.W. Kunkel, Antitumor activity of substituted *E*-3-(3,4,5-trimethoxybenzylidene)-1,3-dihydroindol-2-ones, J. Med. Chem. 49 (2006) 6922–6924.
[7] A. Millemaggi, R.J.K. Taylor, 3-Alkenyl-oxindoles: natural products, pharmaceuticals, and recent synthetic advances in tandem/telescoped approaches, Eur. J. Org. Chem. 4527–4547 (2010).
[8] L. Sun, C. Liang, S. Shirazian, Y. Zhou, T. Miller, J. Cui, J.Y. Fukuda, J.Y. Chu, A. Nematalla, X. Wang, H. Chen, A. Sistla, T.C. Luu, F. Tang, J. Wei, C. Tang, Discovery of 5-[5-Fluoro-2-oxo-1,2- dihydroindol-(3*Z*)-ylidenemethyl]-2,4- dimethyl-1*H*-pyrrole-3-carboxylic acid (2-diethylaminoethyl)amide, a novel tyrosine kinase inhibitor targeting vascular endothelial and platelet-derived growth factor receptor tyrosine kinase, J. Med. Chem. 46 (2003) 1116–1119.
[9] R. Roskoski Jr., Sunitinib: a VEGF and PDGF receptor protein kinase and angiogenesis inhibitor, Biochem. Biophys. Res. Commun. 356 (2007) 323–328.
[10] T.L. Underiner, B. Ruggeri, D.E. Gingrich, Development of vascular endothelial growth factor receptor (VEGFR) kinase inhibitors as anti-angiogenic agents in cancer therapy, Curr. Med. Chem. 11 (2004) 731–745.
[11] Z. Chen, P.J. Merta, N.H. Lin, S.K. Tahir, P. Kovar, H.L. Sham, H. Zhang, A-432411, a novel indolinone compound that disrupts spindle pole formation and inhibits human cancer cell growth, Mol. Cancer Ther. 4 (2005) 562–568.
[12] M. Singhal, A. Paul, H.P. Singh, Design synthesis and biological evaluation of 2-methylphenyl semicarbazone derivatives Singh Bangladesh, J. Pharmacol. 6 (2011) 1–7.
[13] M.P. Narasimharao, B. Nagaraju, J. Kovvuri, S. Polepalli, S. Alavala, M.V.P.S. Vishnuvardhan, P. Swapna, V.D. Nimbarte, J.K. Lakshmi, N. Jain, A. Kamal, Synthesis of imidazo-thiadiazole linked indolinone conjugates and evaluated their microtubule network disrupting and apoptosis inducing ability, Bioorg. Chem. 76 (2018) 420–436.
[14] F. Sultana, S.P. Shaik, V.L. Nayak, S.M.A. Hussaini, K. Marumudi, B. Sridevi, T.B. Shaik, D. Bhattacharjee, A. Alarifi, A. Kamal, Design, synthesis and biological evaluation of 2-anilinopyridyl-linked oxindole conjugates as potent tubulin polymerisation inhibitors, Chem. Select 2 (2017) 9901–9910.
[15] A. Kamal, A.B. Shaik, N. Jain, C. Kishor, A. Nagabhushana, B. Supriya, G. Bharath Kumar, S.S. Chourasiya, Y. Suresh, R.K. Mishra, A. Addlagatta, Eur. J. Med. Chem. 92 (2015) 501–513.
[16] V. Naidu, U.M. Bandari, A.K. Giddam, K.R.D. Babu, J. Ding, K.S. Babu, B. Ramesh, R.R. Pragada, P. Gopalakrishnakone, Apoptogenic activity of ethyl acetate extract of leaves of Memecylon edule on human gastric carcinoma cells viamitochondrial dependent pathway, Asian Pac. J. Trop. Med. 6 (2013) 337–345.
[17] P.V.S. Ramya, et al., Synthesis and biological evaluation of curcumin inspired imidazo[1,2-a]pyridine analogues as tubulin polymerization inhibitors, Eur. J. Med. Chem. 143 (2018) 216–231.
[18] A. J Vallejo, L. Salazar, and M. Grijalv, Oxidative stress modulation and ROS-mediated toxicity in cancer: a review on in vitro models for plant-derived compounds 2017, 4586068, 9.
[19] F. Sultana, B. Srinivasa Reddy, V. Ganga Reddy, V. Lakshma Nayak, R.K. Akunuri, R. Sunitha Rani, A. Alarifi, M.S.K. Halmuthur, A. Kamal, Synthesis of benzo[d] imidazo[2,1-b]thiazole-chalcone conjugates as microtubule targeting and apoptosis inducing agents, Bioorg. Chem. 76 (2018) 1–12.
[20] B.R. Acharya, S. Bhattacharyya, D. Choudhury, G. Chakrabarti, The microtubule depolymerizing agent naphthazarin induces both apoptosis and autophagy in A549 lung cancer cells, Apoptosis 16 (2011) 924–939.
[21] D. Choudhury, P.L. Xavier, K. Chaudhari, R. John, A.K. Dasgupta, T. Pradeep, Gopal Chakrabarti, Unprecedented inhibition of tubulin polymerization directed by gold nanoparticles inducing cell cycle arrest and apoptosis, Nanoscale 5 (2013) 4476–4489.
[22] M. Liu, X. Zhao, J. Zhao, L. Xiao, H. Liu, C. Wang, L. Cheng, N. Wu, X. Lin, Induction of apoptosis, G0/G1 phase arrest and microtubule disassembly in K562 leukemia cells by Mere15, a novel polypeptide from *Meretrix meretrix* Linnaeus, Mar. Drugs 10 (2012) 2596–2607.
[23] R. Kaur, et al., Recent developments in tubulin polymerization inhibitors. An overview, Eur. J. Med. Chem. 87 (2014) 89e124.
[24] P.V.S. Ramya, S. Angapelly, L. Guntuku, C.S. Digwal, B.N. Babu, V.G.M. Naidu, A. Kamal, Eur. J. Med. Chem. 127 (2017) 100–114.
[25] Schrödinger suite 2014-3; Schrödinger, LLC, New York, 2014.
[26] C. Maria, M. Zofia, J.M. Chrzanowska, G.K. Andrzej, Synthesis and crystal structure of (4s)-4-benzyl-3-(4,5-dimethoxy-2-methylbenzoyl)-2,2-dimethyl-1,3-oxazolidine, Heterocycles 90 (2015) 730–739.
[27] N. Jain, D. Yada, T.B. Shaik, G. Vasantha, P.S. Reddy, S.V. Kalivendi, B. Sreedhar, Synthesis and antitumor evaluation of nitrovinyl biphenyls: anticancer agents based on allocolchicines, Chem. Med. Chem. 6 (2011) 859–868.
[28] N.P. Kumar, T. Sowjanya, T. Ramya, S.S. Kumari, U.J. Lakshmi, G. Chandraiah, N. Shankaraiah, A. Kamal, Sulfamic acid promoted one-pot synthesis of phenanthrene fused-dihydrodibenzo-quinolinones: anticancer activity, tubulin polymerization inhibition and apoptosis inducing studies 26 (2018) 1996–2008.
[29] T. Ramya, S. Bale, I.P. Janrao, A. Vennela, N.P. Kumar, K.R. Senwar, G. Chandraiah, N. Shankaraiah, Synthesis of 1,2,4-triazole-linked urea/thiourea conjugates as cytotoxic and apoptosis inducing agents, Bioorg. Med. Chem. Lett. 28 (2018) 1919–1924.